Chapter 2

Theory - SBRC fundamentals

The approach proposed to estimate hydraulic properties of rocks using microseismicity is called "Seismicity Based Reservoir Characterization" (SBRC). It uses a spatio-temporal analysis of fluid-injection induced microseismicity to reconstruct the tensor of hydraulic diffusivity and to estimate the tensor of permeability (see Shapiro et al. [1997, 1999a, 2000b] and the discussion of the method in Cornet [2000]). The approach assumes the following main hypothesis: Fluid injections in boreholes cause perturbations of the pore pressure in rocks. Such perturbations cause a change of the effective stress, which, if large enough, can trigger earthquakes along pre-existing zones of weakness. The SBRC approach considers that most of the seismicity is triggered along critically stressed, pre-existing fractures.

Furthermore, the SBRC method assumes that the spatio-temporal evolution of the hydraulically-induced microseismicity is completely defined by the diffusion-like process of pore-pressure relaxation. The analysis of spatio-temporal features of the microseismicity then provides a possibility to invert for hydraulic diffusivity distributions in fluid-saturated rocks.

In the low-frequency limit of the Biot equations of poroelasticity (Biot [1962]) the pore-pressure perturbation p can be approximately described by the differential equation of diffusion. In this equation, the hydraulic diffusivity tensor D_{ij} is the dominant parameter. The tensor of hydraulic diffusivity is directly proportional to the tensor of permeability (see Shapiro et al. [2002]).

2.1   The concept of triggering fronts

In the following a real configuration of a fluid injection in a borehole is approximated by a point source of pore pressure perturbation in an infinite heterogeneous anisotropic poroelastic fluid-saturated medium. In the low-frequency limit of the Biot equations (Biot

[1962]) the pore-pressure perturbation p can be approximately described by the following differential equation of diffusion:

$$\frac{\partial p}{\partial t} = \frac{\partial}{\partial x_i} \left[D_{ij} \frac{\partial}{\partial x_j} p \right],$$ (2.1)

where D_{ij} are components of the tensor of the hydraulic diffusivity, x_j ($j = 1, 2, 3$) are the components of the radius vector from the injection point to an observation point in the medium and t is the time. This equation corresponds to the second-type Biot waves (the slow P-waves) in the low frequency limit and describes linear relaxation of pore-pressure perturbations. Note, that this equation is valid for a heterogeneous medium in respect of its hydraulic properties. In other words, components of the tensor of the hydraulic diffusivity can be heterogeneously distributed in the medium. The tensor of hydraulic diffusivity is directly proportional to the tensor of permeability and this is discussed later (see eq. 2.21).

In some situations (e.g., some hydrofracturing experiments) the hydraulic diffusivity can be changed considerably by the fluid injection. This means, that in the equation above the diffusivity tensor must become pore-pressure dependent. Therefore, this equation becomes non-linear. Such changes of the diffusivity take place in restricted regions around boreholes. However, the aim of the SBRC method is to estimate the effective hydraulic diffusivity in a large rock volume of the spatial scale of the order of about one kilometer and more. Generally, estimates of hydraulic diffusivity are able for the whole seismically active volume of rock.

Because even small pore-pressure fluctuations are able to trigger microseismicity (see e.g., Zoback and Harjes [1997a] and Shapiro et al. [1997]) it is natural to assume that in a given elementary volume of the medium, the triggering of the earliest microseismic events starts before the substantial relaxation of the pore-pressure occurs. This means, that even in the 'near zone' very early events occur in the practically unchanged medium. In other words, the front of significant changes of the medium propagates behind the quicker triggering front of earlier microseismic events. However, it is precisely these early events that are important for our approach for estimating the diffusivity. Thus, the corresponding estimate should be approximately equal to the diffusivity of the unchanged medium even in such situations, where the diffusivity was strongly enhanced by the hydraulic fracturing. Because of this reason it is assumed that changes of the diffusivity caused by the injection can be neglected. Thus, D_{ij} is assumed to be pressure independent in eq. (2.1).

In figure 2.1 an example of a cloud of events is shown collected in December 1983 during the hydraulic injection into crystalline rock at a depth of 3463 meters at the Fenton Hill (USA) geothermal energy site (see for details and further references Fehler et al. [1998]). Injection took place for about 80 hours at a depth of approximately 3.5 km. About 11366 events were induced. The lateral as well the vertical extension of the cumulative cloud was about 1 km. Color correspond to the event occurrence times after the start of the injection. The solid line corresponds to the injection borehole. Obviously, the events occurring early after the fluid injection was started are located around the source location. Events occurring later are located farther away from the borehole. This makes clear, that the cloud of events shows a spatio-temporal evolution character.
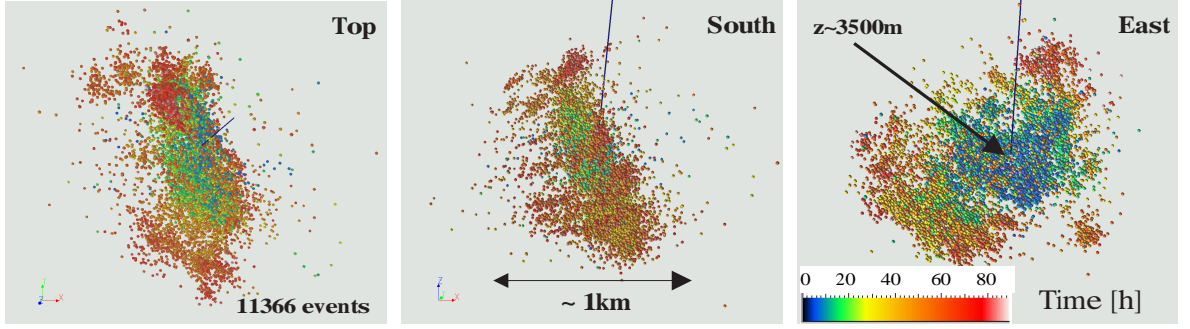
Figure 2.1: Hypocenters of the microseismic events induced during the fluid injection experiments of the Fenton Hill experiment, 1983. Color correspond to the event occurrence times after the start of the injection. The solid line corresponds to the injection borehole.

In figure 2.2 a microseismic cloud induced at the hot-dry-rock geothermal site at Soultz-sous-Forêts (France) in 1993 is shown, where about 18000 events were induced during an injection experiment (see Dyer et al. [1994]). The injection test continued for about 350 hours and fed about 25.300 m^3 of water into the rock at a depth of 2.85-3.0 km. Approximately 9300 of these events were localized with sufficient accuracy within 400 hours after the injection. The seismically active volume of rock comprises approximately 1.5 km^3.
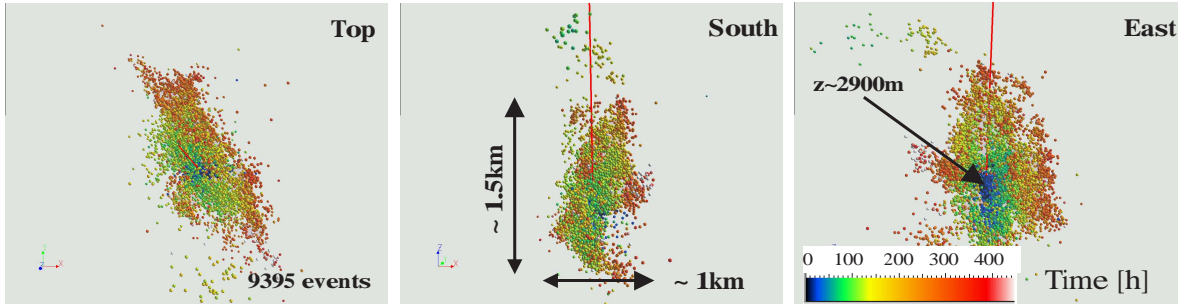

Figure 2.2: Hypocenters of the microseismic events induced during the fluid injection experiments of the Soultz-sous-Forêts experiment, 1993. Color correspond to the event occurrence times after the start of the injection. The solid line corresponds to the injection borehole.

To introduce the concept of triggering fronts in a more formal way let us firstly recall the form of the solution of (2.1) in the case of a homogeneous poroelastic medium. In the case of anisotropic homogeneous medium equation (2.1) takes the following form

$$\frac{\partial p}{\partial t} = D_{ij} \frac{\partial}{\partial x_i} \frac{\partial}{\partial x_j} p. \tag{2.2}$$

If the medium is also isotropic (i.e., $D_{11} = D_{22} = D_{33} = D$, and $D_{ij} = 0$, if $i \neq j$), then

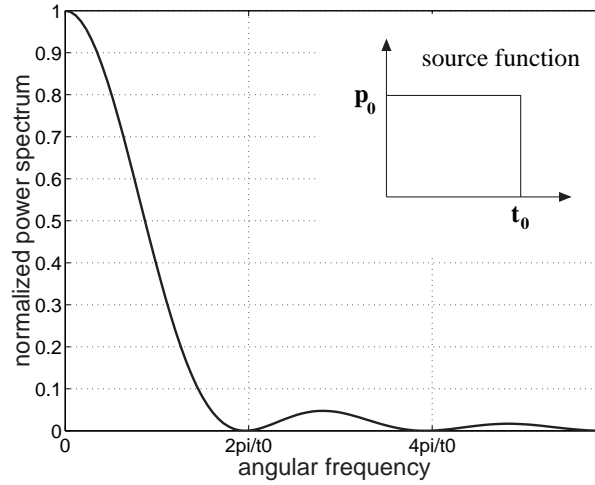$$\frac{\partial p}{\partial t} = D \triangle p, \tag{2.3}$$

Figure 2.3: Power spectrum of an rectangle pulse. The time-function of this pulse is given in the upper right plot in this figure (taken from Shapiro et al. [2002]).

and D is the scalar hydraulic diffusivity. If a time-harmonic perturbation $p_0 \exp(-i\omega t)$ of the pore-pressure perturbation is given on a small spherical surface of the radius a with the center at the injection point, then the solution of equation (2.3) is

$$p(r,t) = p_0 e^{-i\omega t} \frac{a}{r} \exp\left[(i-1)(r-a)\sqrt{\frac{\omega}{2D}}\right], \qquad (2.4)$$

where ω is the angular frequency and $r = |r|$ is the distance from the injection point to the point, where the solution is looked for. From equation (2.4) one note that the solution can be considered as a spherical wave (it corresponds to the slow compressional wave in the Biot theory) with the attenuation coefficient equal to $\sqrt{\omega/2D}$ and the slowness equal to $1/\sqrt{\omega 2D}$.

In reality the pore pressure at the injection point is not a harmonic function. Let us roughly approximate the pore pressure perturbation at the injection point by a step function $p(t) = p_0$, if $t \geq 0$ and $p(t) = 0$ if $t < 0$ (see figure 2.3). For instance, this can be a rough approximation in some cases of a borehole fluid injection (e.g. for a hydraulic fracturing or other fluid tests). For a particular seismic event at the time t_0 the time evolution of the injection signal for the time $t > t_0$ is of no further consequence. Thus, this event is triggered by the rectangular signal $p(t) = p_0$ if $0 \leq t \leq t_0$ and $p(t) = 0$ if $t < 0$ or $t > t_0$. The power spectrum of this signal has the following form:

$$4p_0^2 t_0^2 \frac{\sin^2(\omega t_0/2)}{\omega^2 t_0^2} \qquad (2.5)$$

This is the square of a well known *sinc*-function. A plot of this function for t_0 and p_0 equal 1 is shown on figure 2.3. It is seen that the dominant part of the power spectrum

is located in the frequency range below $2\pi/t_0$. The magnitude of the second maximum is approximately 25 times smaller than those of the first one.

It is natural to assume that the probability of the triggering of microseismic events is an increasing function of the power of the pressure perturbation. Thus, the probability, that the seismic event at the time t_0 was triggered by signal components from the frequency range $\omega \leq 2\pi/t_0$ is high. This probability for the lower energetic high frequency components is small. However, from equation (2.4) one has seen that the propagation velocity of harmonic components of the pressure perturbation is proportional to $\sqrt{\omega}$. Therefore, the velocity of high-frequency components is higher than those of the low frequency components. Thus, to a given time t_0 it is probable that events will occur at distances, which are smaller than the travel distance of the slow-wave signal with the dominant frequency $2\pi/t_0$. The events are characterized by a significantly lower occurrence probability for larger distances. The spatial surface which separates these two spatial domains is called the *triggering front*. It corresponds to the location of the front of zero phase of the harmonic slow wave with the frequency $2\pi/t_0$ at the time t_0.

2.1.1 Triggering fronts in homogeneous anisotropic media

Let us firstly assume, that the medium is homogeneous and isotropic. Then the slowness of the slow wave (see eq. 2.4) can be used to estimate the size of the spatial domain, where microseismic events are characterized by a high probability. One obtains (see also Shapiro et al. 1997)

$$r = \sqrt{4\pi Dt}. \tag{2.6}$$

This is the equation for the triggering front in an effective isotropic homogeneous poroelastic medium with the scalar hydraulic diffusivity D. If the value of the hydraulic diffusivity in equation (2.6) is selected correctly, then equation (2.6) will correspond to the upper bound of the cloud of events in the plot of their spatio-temporal distribution (i.e., the plot of r versus t, called 'r-t plot' in further chapters).

In figure 2.4a a spatio-temporal distribution of the microseismicity according to equation (2.6) is shown for the the microseismic data collected at Fenton Hill. A good agreement between the theoretical curve with $D = 0.17m^2/s$ and the data is seen.

Such a good agreement supporting the above concept of the triggering of microseismicity can be observed in many other cases. For example figure 2.4b shows a similar r-t plot for the microseismic cloud induced at Soultz-sous-Forêts. The diffusivity $D = 0.05m^2/s$ was observed for the seismically-active volume of the crystalline rock at the depth of 2500-3500m.
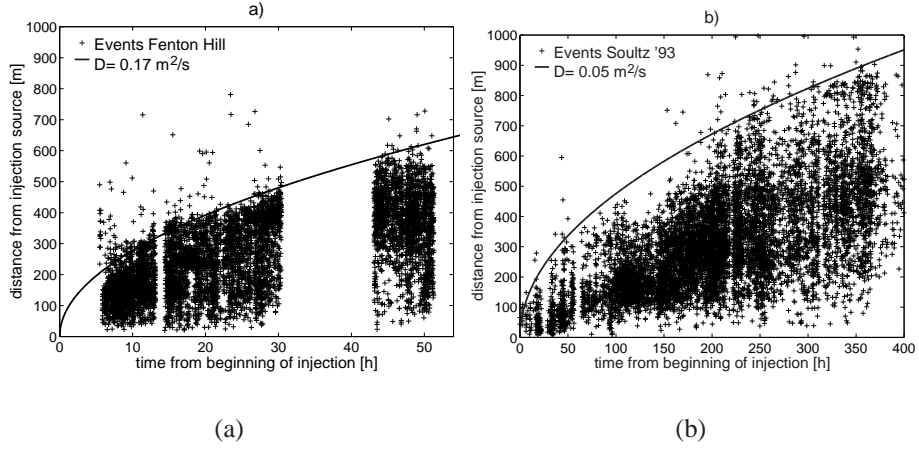
(a)   (b)

Figure 2.4: Distances of events from the injection source versus their occurrence time for a) the Fenton Hill experiment, 1983 and b) the Soultz-sous-Forêts experiment, 1993. Taken from Shapiro et al. [2002].

2.1.2   Diffusivity tensor estimation in 3D

Equation (2.6) provides scalar estimates of D only. Let us now assume, that D_{ij} is homogeneously distributed in the medium. When estimating the diffusivity under such an assumption the complete heterogeneous seismically-active rock volume is replaced by an effective homogeneous anisotropic poroelastic fluid-saturated medium. The permeability tensor of this effective medium is the permeability tensor of the heterogeneous rock upscaled to the characteristic size of the seismically-active region.

Performing very similar consideration as in Shapiro et al. [1997], but now using equation (2.1) for homogeneous but anisotropic media the following equation for the triggering front can be obtained for anisotropic media (Shapiro et al. [1999]):

$$r = \sqrt{\frac{4\pi t}{n^T D^{-1} n}}. \tag{2.7}$$

T denotes that the matrix (vector) is transposed, $n = r/|\bar{r}|$ and D^{-1} is the inverse of D. Let us consider this equation in the principal coordinate system of the diffusivity tensor. Then, the matrix D_{ij} becomes diagonal (D_{11}, D_{22}, D_{33}), and one obtains:

$$\frac{x_1^2}{D_{11}} + \frac{x_2^2}{D_{22}} + \frac{x_3^2}{D_{33}} = 4\pi t. \tag{2.8}$$

If the principal coordinate system is scaled in the following way

$$x_{sj} = \frac{x_j}{\sqrt{4\pi t}}, \tag{2.9}$$

then the equation of the triggering front will be an equation of an ellipsoid:

$$\frac{x_{s1}^2}{D_{11}} + \frac{x_{s2}^2}{D_{22}} + \frac{x_{s3}^2}{D_{33}} = 1 \tag{2.10}$$

with the half-axes equal to the square roots of the principal diffusivities. It is clear that the ellipsoid will keep its shape in an arbitrary rotated coordinate system. Therefore, if the coordinates of all events are scaled by the square root of their occurrence time using equation (2.9) then — by analogy with equation (2.6) and figure 2.3 — the ellipsoid (eq. 2.10) will be an envelope of the cloud of events, but now in a normalized 3-D space.
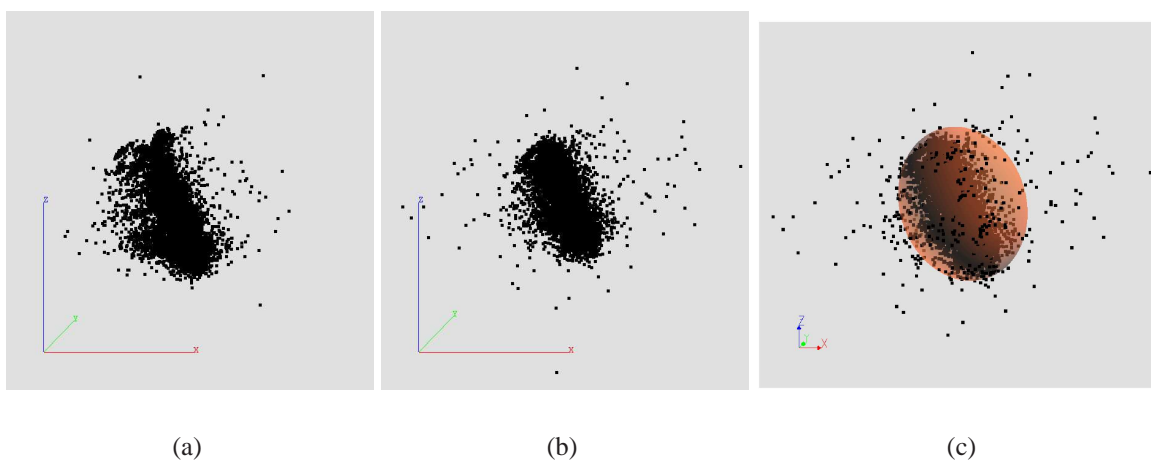

| (a) | (b) | (c) |

Figure 2.5: a) a view of the Fenton Hill microseismicity cloud from the South. b) the same view of the cloud in the coordinate system scaled in accordance with equation (2.9). c) cloud in the scaled coordinate system together with an fitting ellipsoid.
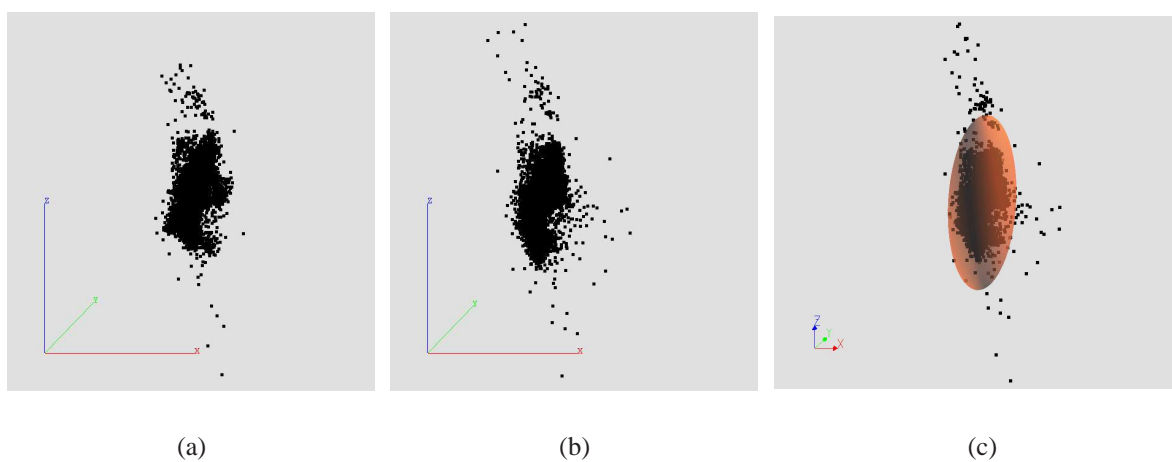

| (a) | (b) | (c) |

Figure 2.6: a) a view of the Soultz microseismicity cloud from the South. b) the same view of the cloud in the coordinate system scaled in accordance with equation (2.9). c) cloud in the scaled coordinate system together with an fitting ellipsoid.

Let us now return to the examples of the Fenton Hill and Soultz HDR experiments to demonstrate this signature of the diffusive nature of the triggering of events. Figure 2.5a shows a view of the Fenton Hill microseismicity cloud from the South. In figure (b) the same view of the cloud in the coordinate system scaled in accordance with equation (2.9). The same is shown in figure 2.6 for the Soultz data set. In both cases one observes that in the scaled coordinate systems (b) the shapes of the microseismic clouds become more similar to ellipsoids than in the original coordinate system. This happens because in reality, locations where rocks are close to a failure equilibrium are randomly distributed in space. Therefore, even if the medium is hydraulically homogeneous, the seismicity cloud can be very irregular. By normalization according to equation (2.9), some irregularities will be eliminated, and the seismicity cloud will tend to an ellipsoid closely related to the diffusivity tensor, as equation (2.10) shows. Of course, all features considered above can be significantly disturbed in strongly heterogeneous hydraulic media. However, as the examples above show, they can be observed in reality. Features of hydraulically induced seismicity considered above are controlled by the diffusivity tensor. This tensor is directly proportional to the tensor of permeability.

The estimation of a hydraulic diffusivity ellipsoid for the Fenton Hill data is shown in figure 2.5c and for the Soultz data in figure 2.6c, respectively. More information about this extension of the method can be found in Rindschwentner [2001] and Shapiro et al. [2003]. For the hydraulic diffusivity tensors shown, following estimates were obtained:

$$\mathbf{D}_{Fenton} = \begin{pmatrix} 5.9 & 0 & 0 \\ 0 & 7.2 & 0 \\ 0 & 0 & 14.2 \end{pmatrix} 10^{-2} \mathrm{m}^2/\mathrm{s}, \qquad \mathbf{D}_{Soultz} = \begin{pmatrix} 1.9 & 0 & 0 \\ 0 & 4.8 & 0 \\ 0 & 0 & 14.2 \end{pmatrix} 10^{-2} \mathrm{m}^2/\mathrm{s}$$

The values found correlate well with results of independent studies and diffusivity/permeability estimates at these sites (Rindschwentner [2001]).

2.1.3   Group-velocity surface of anisotropic slow waves

To gain more insight into the physical nature of the triggering-front surface (eq. 2.7) solutions of the anisotropic diffusion equation are considered (2.2) in the form of homogeneous plane waves:

$$e^{\left(ik_j x_j - i\omega t\right)}. \tag{2.11}$$

Because we look for homogeneous waves (i.e. the real and imaginary parts of the wave vector are parallel) a unit vector e in the direction of the wave vector k can be defined:

$$k = e\left(a + ib\right) = ek, \tag{2.12}$$

where a and b are real numbers and k is a complex one. Substituting equation (2.11) into the diffusion equation (2.2) one obtains the following dispersion relationship characterizing the low-frequency propagation of slow waves:

$$\omega = -iD_{lm}k_lk_m = -iD_{lm}e_le_mk^2. \qquad (2.13)$$

This equation gives

$$|k^2| = \frac{|\omega|}{D_{gs}e_ge_s}. \qquad (2.14)$$

The dispersion equation provides us with the following group velocity of anisotropic low-frequency slow waves (see the definition of the group velocity in Landau and Lifshitz [1984]):

$$V_j^{gr} = \frac{\partial \omega}{\partial k_j} = -iD_{lm}(k_l\delta_{mj} + k_m\delta_{lj}) = -2iD_{lj}k_l = -2iD_{lj}e_lk, \qquad (2.15)$$

This gives the following absolute value of the group velocity:

$$
\begin{aligned}
|V^{gr}|^2 &= V_j^{gr\star}V_j^{gr} \\
&= -2iD_{lj}e_lk \cdot 2iD_{mj}e_mk^* \\
&= 4D_{lj}D_{mj}e_le_m|k|^2 \\
&= 4D_{lj}D_{mj}e_le_m\frac{|\omega|}{D_{gs}e_ge_s} \\
&= 4|\omega|\frac{e^TDDe}{e^TDe},
\end{aligned} \qquad (2.16)
$$

In turn, eq. (11) shows that the direction of the group velocity is defined by a unit vector e^{gr} with the components:

$$e_j^{gr} = D_{lj}e_l / \sqrt{D_{gm}e_gD_{sm}e_s}. \qquad (2.17)$$

Therefore,

$$e^{gr} = \frac{De}{e^TDDe} \qquad (2.18)$$

Using the property of diagonal symmetry of the tensor of hydraulic diffusivity, inverting this equation and changing the notations so that: $e^{gr} = n$ one finally arrives at the following result:

$$|V^{gr}| = \sqrt{\frac{4|\omega|}{n^T D^{-1} n}}. \qquad (2.19)$$

A comparison of equations (2.7) and (2.19) shows that the triggering front has the same spatial form as the group-velocity surface of anisotropic slow waves. Physically this means that in the case of a point injection source triggering fronts in anisotropic rocks propagate like heat fronts or light fronts in anisotropic crystals.

2.1.4 Inversion for the global diffusivity and permeability tensors

Shapiro et al. [1999a] proposed the following approach for estimating the diffusivity tensor using equation (2.7). The entire space is divided in M directional sectors centered at the injection point. In each spatial sector the hydraulic diffusivity is estimated using equation (2.6). Thus, M values of the hydraulic diffusivity are estimated for M different sectors of the space. They are called *directional diffusivities D_i*. The directional diffusivity D_i approximately characterizes the process of the pore-pressure relaxation along the direction n_i, given by the central ray of i-th sector. On the other hand, the triggering front in an anisotropic medium is described by equation (2.7).

Thus, the following system of matrix equations can be obtained from equations (2.6) and (2.7):

$$n_i^T D^{-1} n_i = 1/D_i, \quad for \quad (i = 1,...,M). \qquad (2.20)$$

This system can be solved in a least squares sense. Using this approach not only the diffusivity tensor but also errors of its estimations can be obtained. For example, in the case of the above mentioned Soultz experiment the error of estimates of the principal components is of the order of 20-30 per cent. Another approach to the inversion for the global diffusivity tensor was proposed in Shapiro et al. [1999b].

The relationship between the hydraulic diffusivity and the permeability is derived along with equation (2.1). For this Darcy's law must be combined with the equation of mass conservation (see e.g., Mavko et al. [1998], Section 8.1). In such derivations different authors use different notations, arriving of course to analogous relationships. For example, Rice and Cleary [1976] and van der Kamp and Gal [1983] use notations of early papers of Biot, e.g., Biot [1956a]. Here we follow notations of Biot [1962] which are broadly used in seismics of poroelastic media. Equation (2.1) is directly derived as low-frequency limit of the system of Biot equations (Biot [1962]) describing acoustics of poroelastic systems. This derivation can be found in Dutta and Ode [1979]. Moreover, Dutta and Ode [1979] show that equation (2.1) characterizes the low-frequency slow wave. Assuming that the poroelastic continuum is isotropic and homogeneous relative to all its elastic parameters and porosity, and that only the permeability can be anisotropic and heterogeneously

distributed, equations (60), (62) and (63) of Dutta and Ode [1979] provide equation (2.1) along with the following relationship between the hydraulic diffusivity and permeability:

$$D = NK/\eta, \tag{2.21}$$

where K is the permeability tensor, η is the pore-fluid dynamic viscosity and N is a poroelastic modulus defined as follows: $N = MP_d/H; M = (\phi/K_f + (\alpha - \phi)/K_g)^{-1}; \alpha = 1 - K_d/K_g; H = P_d + \alpha^2 M; P_d = K_d + 4/3\mu_d$. Here $K_{f,d,g}$ are bulk moduli of the fluid, dry frame and grain material respectively; μ_d is the shear modulus of the frame and ϕ is the porosity. Note also, that here the elastic anisotropy in comparison with the anisotropy of the permeability is neglected. For the case of a highly porous rocks an approximation $N \approx K_f/\phi$ can be used. For the case of low-porosity crystalline rocks N can be approximated as follows: $N = \left[\phi/K_f + \alpha/K_g\right]^{-1}$.

For example, for the Fenton Hill experiment, accepting the following estimates used in the literature for the crystalline rock at the depth of 3500m: $\phi = 0.003$, $\eta = 1.9 \cdot 10^{-4}$ Pa.sec. (dynamic viscosity of salt water at 150°C), $K_d = 49$ GPa, $K_g = 75$ GPa and $K_f = 2.2$ GPa one obtains $N \approx 1.68 \ 10^{11}$ Pa, and the permeability tensor in the principle coordinate system is:

$$\mathbf{K} = \begin{pmatrix} 0.2 & 0 & 0 \\ 0 & 0.8 & 0 \\ 0 & 0 & 1.8 \end{pmatrix} 10^{-16} m^2 \tag{2.22}$$

It is important to note that usually the permeability estimates of the SBRC are in a good agreement with independent results of different hydraulic tests. Hydraulic tests in Fenton Hill show estimates of the large-scale permeability of the order of $10^{-17} - 10^{-15} m^2$ (M. Fehler, personal communication). Similar experiments in Soultz provided the following estimates:

$$\mathbf{K} = \begin{pmatrix} 0.7 & 0 & 0 \\ 0 & 1.9 & 0 \\ 0 & 0 & 5.2 \end{pmatrix} 10^{-17} m^2 \tag{2.23}$$

2.2 Triggering fronts in heterogeneous media

To demonstrate the idea of the 3-D mapping of hydraulic diffusivity let us consider the microseismicity cloud collected during the Soultz experiment mentioned above.

Figure 2.7 shows a view of this cloud. For each event the color shows its occurrence time in respect to the start time of the injection. Evidently, the occurrence times contain much more information than just the large-scale global velocity of the triggering front propagation in an effective homogeneous anisotropic medium. If the space is subdivided to a number of 3-D cells an arrival time of the triggering front can be defined into each of these cells. Under such an arrival time one can understand a minimum occurrence time in a given cell. After
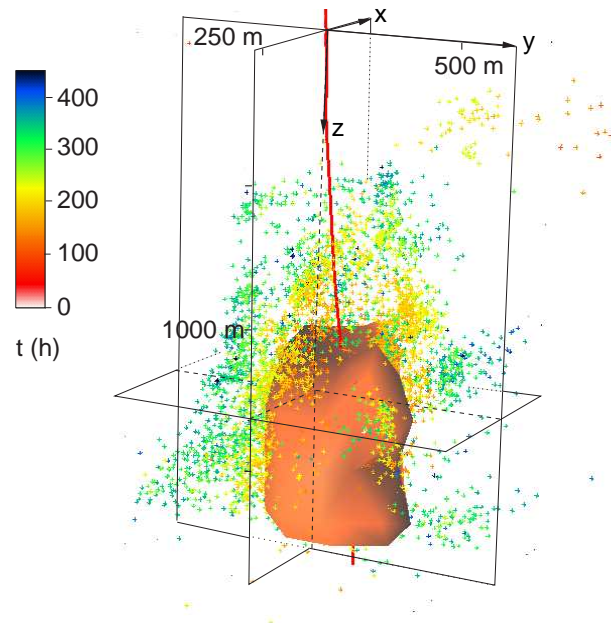
Figure 2.7: A perspective projection of the 3-D distribution of microseismic events registered during the Soultz-sous-Forêts experiment: Borehole GPK1, September 1-22, 1993. The color corresponds to the event occurrence time. The axes X,Y and Z point to the East, the North and the earth surface, respectively. The vertical and horizontal sizes of the shown spatial frame $(X \times Y \times Z)$ are $802.5m \times 1274m \times 1943m$. The depth of the frame's bottom is $3503m$. The surface shown is the triggering front of microseismicity for the arrival time of 100h. The vertical and horizontal scales of the figure are equal.

some smoothing and interpolation the triggering fronts can be constructed for given arrival times. Figure 2.7 also shows such a triggering front for the arrival times of 100h. It is clear, that such a surface can be constructed for any arrival time presented in microseismic data. Thus, the triggering front propagation can be observed. In a heterogeneous porous medium the propagation of the triggering front is determined by its heterogeneously distributed velocity. Given the triggering front positions for different arrival times, the 3-D distribution of the propagation velocity can be reconstructed. In turn, the hydraulic diffusivity is directly related to this velocity.

In the following it is tried to formalize this concept. As discussed above, the propagation of the triggering front is approximately defined by kinematic features of a slow-wave front of a particular frequency (see also later eq. 2.29). For the SBRC approach the earliest microseismic events are of importance. It is natural to assume, that for their triggering in a heterogeneous medium a possibly quickest front configuration will be responsible.

On the other hand, in the low-frequency range the slow wave represents the process of the pore pressure relaxation and, therefore, is a kind of a diffusion wave. The real and imaginary parts of its wave vector are equal. Thus, it is a very rapidly attenuating wave.

However, recent studies of diffusion waves (more systematic studies were performed for a particular type of diffusion waves called the diffuse photon-density waves: see Yodh and Chance [1995]; Boas et al. [1997] and further references there; Mandelis [2000] found that

they show all typical wave phenomena, like scattering, diffraction, refraction, reflection etc.. Though different in character and aims, similar approaches are known from the field of diffusive (i.e. low frequency) electromagnetics. Several techniques have been developed to use wave techniques on these kind of data (Nekut [1994]; Gibert et al. [1994]; Virieux et al. [1994]). Similar methods are also used in thermal-wave imaging (Pad*é* [1994] and the references given there).

This argumentation leads to the idea to use a geometrical-optics like description of triggering fronts as an approximative basis for the microseismic data inversion.

2.2.1 Triggering fronts for the case of a quasi-harmonic pressure perturbation

In the following we shall consider relaxation of a harmonic component of a pressure perturbation. By analogy with (2.4) we will look for the solution of equation (2.1) in a similar form:

$$p(r,t) = p_0(r)e^{-i\omega t} \exp\left[\sqrt{\omega}\tau(r)\right], \tag{2.24}$$

It is also assumed that $p_0(r)$, $\tau(r)$ and $D_{ij}(r)$ are functions slowly changing with r.

Substituting equation (2.24) into equation (2.1), accepting ω as a large parameter and keeping only terms with largest powers of ω (these are terms of the order $O(\omega)$; the other terms, which are of the orders $O(\omega^0)$ and $O(\omega^{1/2})$ are neglected) one obtains the following equation:

$$-i = D_{ij}\frac{\partial\tau}{\partial x_i}\frac{\partial\tau}{\partial x_j}. \tag{2.25}$$

Considering again the homogeneous-medium solution (2.4) it can be concluded that the frequency-independent quantity τ is related to the frequency-dependent phase travel time T as follows:

$$\tau = (i-1)\sqrt{\omega}T. \tag{2.26}$$

Note, that in turn $T \propto 1/\sqrt{\omega}$. Substituting equation (2.26) into equation (2.25) one obtains:

$$1 = 2\omega D_{ij}\frac{\partial T}{\partial x_i}\frac{\partial T}{\partial x_j}. \tag{2.27}$$

In the case of an isotropic poroelastic medium $D_{ij} = \delta_{ij}D$, and equation (2.27) is reduced to the following one:

$$|\nabla T|^2 = \frac{1}{2\omega D}. \tag{2.28}$$

Thus, a standard eikonal equation has been obtained. The right hand part of this equation is the squared slowness of the slow wave. One can show (Červeny [1985]) that equation (2.28) is equivalent to the Fermat's principle which ensures the minimum time (stationary time) signal propagation between two points of the medium. Due to equation (2.26) the minimum travel time corresponds to the minimum attenuation of the signal. Thus, in this sense, equation (2.28) describes the minimum-time maximum-energy front configuration.

2.2.2   Triggering fronts in the case of a step-function like pressure perturbation

Let us now return to a more realistic situation, where the pressure perturbation can be roughly approximated by a step function in the source point.

In the previous section an equation for the triggering time $T(r)$ of a harmonic pressure perturbation was derived. Using this equation another one can be derived, which will describe the triggering time $t(r)$ of a step-function pressure perturbation. From our earlier discussion it is known, that the triggering time t roughly corresponds to the frequency

$$\omega_0 = 2\pi/t. \tag{2.29}$$

Thus,

$$T|_{\omega=\omega_0} = t. \tag{2.30}$$

On the other hand, it is known that generally $T(\omega) \propto \sqrt{1/\omega}$. Now this relationship can be used to compute T at the frequency ω_0, if T is known at any arbitrary frequency ω:

$$t = T(\omega_0) = T(\omega)\sqrt{\frac{\omega}{\omega_0}}. \tag{2.31}$$

Using this equation and equation (2.29) one obtains:

$$T(\omega) = \sqrt{\frac{2\pi t}{\omega}}. \tag{2.32}$$

Substituting this equation into equations for T of the previous section one obtains the following results. In the general case of an anisotropic heterogeneous poroelastic medium

$$t = \pi D_{ij}\frac{\partial t}{\partial x_i}\frac{\partial t}{\partial x_j}. \tag{2.33}$$

In the case of an isotropic poroelastic medium this equation is reduced to the following one:

$$D = \frac{t}{\pi |\nabla t|^2}. \tag{2.34}$$

As well as the previous versions of the SBRC the last two equations are also limited to the low-frequency diffusion type of Biot slow waves. The advantage of the last two equations over the previous versions of the SBRC is following. These equations can serve as a basis for an inversion procedure aimed to reconstructing spatial distributions of the hydraulic diffusivity in heterogeneous media. In contrast to this, the previous versions of the SBRC worked with an assumption of a homogeneous medium.

2.2.3 Inversion for the permeability of heterogeneous media

In the case of an isotropic poroelastic medium equation (2.34) can be directly used to reconstruct the 3-D heterogeneous field of the hydraulic diffusivity. In turn, using equation (2.33) in the case of an anisotropic medium, it is impossible to reconstruct a 3-D distribution of the diffusivity tensor. The only possibility is the following. Let us assume that the orientation and the principal components proportion is constant in the medium. Then, the tensor of hydraulic diffusivity can be expressed as

$$D_{ij}(r) = d(r)\xi_{ij}, \tag{2.35}$$

where ξ_{ij} is a nondimensional constant tensor of the same orientation and principal-component proportion as the diffusivity tensor, and d is the heterogeneously distributed magnitude of this tensor. This tensor can be found using the global SBRC estimate of the hydraulic diffusivity as was mentioned above. Then, the quantity d can be directly computed as follows:

$$d = \frac{t}{\pi \xi_{ij} \frac{\partial t}{\partial x_i} \frac{\partial t}{\partial x_j}}. \tag{2.36}$$

Note, that if the tensor ξ_{ij} is normalized so that $\xi_{11} + \xi_{22} + \xi_{33} = 3$, then in the case of an isotropic medium it is equal to the unit matrix. In addition, a transformation of the hydraulic diffusivity tensor to the permeability tensor can be performed using for example equation (2.21) above.

Let us finally consider an example of application of the method. Figure 2.8 shows the reconstructed hydraulic diffusivity for Soultz-1993 data set according to equation (2.34). From the other hand assuming, that the tensor ξ_{ij} has the same orientation and principal-component proportion as the diffusivity tensor given in equation (16) of Shapiro et al. [1999a], equation (2.36) can be applied to obtain the diffusivity-tensor magnitude.
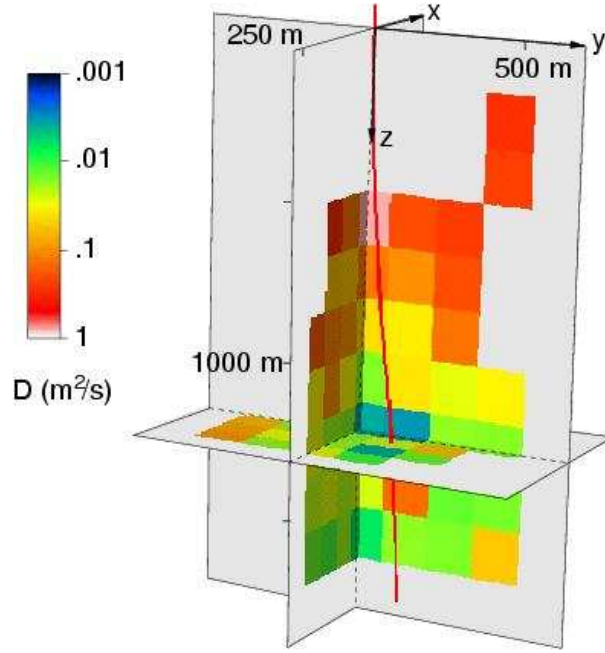
Figure 2.8: An example of the hydraulic diffusivity reconstruction in 3-D for the Soultz-1993 data set. For the inversion isotropic variant of the method has been used. The diffusivity is given in the logarithmic scale. It changes between 0.001 and 1.0 m^2/s. Light gray corresponds to cells with no diffusivity value resolved. The geometry corresponds to that given in figure 2.7.

Without showing this into detail, it is interesting to note that there is no significant difference between the representation of the isotropic and anisotropic variant of the method. They both show larger diffusivity in the upper part of the medium then of the lower one. In addition, a high permeable channel leading to the upper right-hand part of the medium is visible in the reconstructed hydraulic diffusivity. This is in good agreement with figure 2.7, which shows a number of early events in the upper right-hand corner of the rock volume.

2.3   Discussion

The main limitations of the extension of the SBRC to the case of heterogeneous media proposed here are apparently related to the validity range of equation (2.25). Roughly they can be formulated from the following consideration of the right hand part of equation (2.1) in a 1-D medium:

$$\frac{\partial}{\partial x}\left[D\frac{\partial p}{\partial x}\right] = \frac{\partial D}{\partial x}\frac{\partial p}{\partial x} + D\frac{\partial^2 p}{\partial x^2} \tag{2.37}$$

Our approach is expected to be valid if the following inequality is satisfied:

$$\frac{\partial D}{\partial x}\frac{\partial p}{\partial x}\bigg|/|D\frac{\partial^2 p}{\partial x^2}| \ll 1 \tag{2.38}$$

This can be roughly reduced to the following: $|\frac{\partial D}{\partial x}|/|Dk| \ll 1$, where k is the wave number. Taking into account that approximately $|k|^2 = \omega/D$ we arrive at the following, rather simplified condition:

$$\frac{|\partial D/\partial x|^2}{D} < \omega. \tag{2.39}$$

This inequality relates the gradient of the hydraulic diffusivity and the frequency of the pressure perturbation. It is rather typical for the geometric optic approximation. It shows, that if the frequency is high enough and the medium heterogeneity is smooth the above approximation can be applied. In the case of the step-function like pressure perturbation the frequency corresponding to the triggering front is accepted to be $\omega = 2\pi/t$. Using the equation of the triggering front in homogeneous poroelastic media (2.6) the occurrence time of earlier events can be roughly approximated as $t \approx x^2/(4\pi D)$. Note, that x denotes the distance from the injection source. Thus, inequality (2.39) can be reduced to the following one

$$\frac{|\partial D/\partial x|}{D} \ll \frac{2\pi\sqrt{2}}{x}. \tag{2.40}$$

This condition is a rather restrictive one. In addition, it shows that the smaller the distance x the higher is the resolution of the method.

In spite of the restrictive character of the inequalities above, the geometric optic approximation is applicable to the propagation of microseismicity triggering fronts under rather common conditions. This is based on the causal nature of the triggering front definition. When considering the triggering front we are interested in a quickest possible configuration of the phase travel time surface for a given frequency. Thus, kinematic aspects of the front propagation are of interest only. The quickest possible configuration of the phase front is usually given by the Hamilton-Jacobi, i.e., eikonal equation. However, the conditions above necessarily take into account not only kinematic aspects of the front propagation but rather mainly dynamic aspects, i.e., amplitude of the pressure perturbation. In other words, the eikonal equation is usually valid in much broader domain of frequencies than those given by the inequalities above. Therefore, the method will give meaningful and useful results, at least semi qualitatively.

2.4 Conclusions

A new technique (SBRC) was developed for reconstructing the permeability distribution in 3-D heterogeneous poroelastic media. For this the seismic emission (microseismicity) induced by a borehole-fluid injection is used. The SBRC is based on the hypothesis that the early triggering front of the hydraulic-induced microseismicity in naturally stressed rocks propagates like a diffusive process (the pore pressure relaxation process) in a heterogeneous anisotropic poroelastic fluid-saturated medium.

In a homogeneous medium the surface of the seismicity triggering front has the same form as the group-velocity surface of the low-frequency anisotropic Biot slow wave. A version of the SBRC approach which assumes that the medium is homogeneous provides an effective (global) permeability tensor upscaled to the characteristic size of the seismically-active heterogeneous rock volume. Usually, global estimates of permeabilities obtained by SBRC agree well with permeability estimates from independent hydraulic observations.

A further generalization of the SBRC approach uses a geometrical-optic approximation for propagation of triggering fronts in heterogeneous media. In this approximation in the case of quasi harmonic pressure perturbations kinematical aspects of triggering front propagation are described by an eikonal equation. This equation must be modified for the case of step-function like perturbation. In the case of isotropic heterogeneous media the inversion for the hydraulic properties of rocks follows from a direct application of this modified eikonal equation. In the case of an anisotropic heterogeneous medium only the magnitude of a global effective permeability tensor can be mapped in a 3-D spatial domain. Results of field examples show that SBRC can be used at least semi-quantitatively to characterize reservoirs. It can be very helpful as a method providing important constrains or starting models to reservoir simulations or for more sophisticated inversions.